Available online at www.sciencedirect.com
SCIENCE DIRECT®
ELSEVIER
International Journal of Solids and Structures 41 (2004) 7155–7180
INTERNATIONAL JOURNAL OF SOLIDS and STRUCTURES
www.elsevier.com/locate/ijsolstr

Imperfection sensitivity of thin elastic cylindrical shells subject to partial axial compression

C.Y. Song [a], J.G. Teng [a,*], J.M. Rotter [b]

[a] Department of Civil and Structural Engineering, The Hong Kong Polytechnic University, Hong Kong, China
[b] Institute for Infrastructure and Environment, School of Engineering and Electronics, Edinburgh University, UK

Received 22 April 2003; received in revised form 14 May 2004
Available online 3 July 2004

Abstract

The paper addresses the buckling of an elastic cylinder under non-uniform axial compression applied at one boundary. It presents a systematic numerical investigation of the nonlinear load carrying behavior and imperfection sensitivity of the shell when a non-uniform axial load is applied to one end in the form of two equal-length uniformly loaded zones, diametrically opposite each other. Four imperfection forms are examined: the linear bifurcation mode, the nonlinear buckling mode, several post-buckling deformed shapes for the perfect shell, and a weld depression. Additional aspects, such as the influence of the weld depression position and its wavelength are also investigated. Special attention is given to the mesh convergence study and the sign of the imperfection amplitude. The numerical results demonstrate that the mode of the lowest linear bifurcation load is not always the 'worst' imperfection form. It is also shown that the critical position for a weld depression can be approximately located by examining the nonlinear buckling mode of the perfect shell and that the weld depression generally causes the lowest buckling load for this load case.

Keywords: Buckling; Postbuckling; Shell; Axial compression; Imperfection sensitivity; Non-uniform; Partial axial compression; Local loads; Elastic

1. Introduction

Cylindrical shells used in civil engineering applications are often subject to very non-uniform axial compressive stresses (Rotter, 1985, 1998), but very little research has been conducted on the failure criteria to which they should be designed. Most of the existing relevant work examined only the linear bifurcation buckling behavior of a perfect shell (Teng, 1996; Teng and Rotter, 2004). Many civil engineering shells (silos, tanks and digesters) are very thin, so the design is controlled by elastic buckling. Cylinders under uniform axial compression have been widely studied, but non-uniform axial loading has received much less

* Corresponding author. Tel.: +852-2766-6012; fax: +852-2334-6389.
E-mail address: cejgteng@polyu.edu.hk (J.G. Teng).

0020-7683/$ - see front matter © 2004 Elsevier Ltd. All rights reserved.
doi:10.1016/j.ijsolstr.2004.05.040

attention. Cylinders under global bending have received some study (Lundquist, 1935; Flügge, 1973; Seide and Weingarten, 1961; Stephens and Starnes, 1975; Antoine, 2000), but the circumferential variation of membrane stress is so slow that the behavior is rather similar to that under uniform compression. Wind-loaded cylinders, which develop non-uniform axial compression have also received some attention (Greiner and Derler, 1995), but very limited information exists on the buckling, nonlinear and post-buckling behavior of imperfect cylindrical shells subject to more general patterns of non-uniform axial compressive stress (Libai and Durban, 1977; Peter, 1974; Saal, 1982; Rotter, 1985; Cai et al., 2002). Some studies of the load-carrying capacity of column-supported shells have recently been undertaken (e.g. Guggenberger et al., 2000), but these relate to failure above supports rather than buckling within the shell. The studies of Cai et al. (2002, 2003) used similar analyses to explore a problem similar to that of the present paper, but adopts a rather different load case, so that these two studies are complimentary. This paper is concerned with the buckling of elastic imperfect cylinders under well-defined local axial compression.

The European standard on shell buckling (ENV 1993-1-6, 1999) requires that when a geometrically nonlinear shell analysis with explicit representation of imperfections is used for design, a range of potentially damaging imperfection forms should be explored. But it gives little guidance on the forms that these damaging imperfections may take. The main aim of this study is to explore the effect of several potentially damaging geometric imperfection forms, under a load case that is significantly different from uniform compression, and well related to the more complex stress states that occur in practical civil engineering structures. The results may then be used to assist in determining the appropriate equivalent imperfections to use in design evaluations using nonlinear buckling analyses for cylindrical shells under different patterns of non-uniform axial compression.

To this end, this paper describes a systematic numerical investigation into the nonlinear elastic behavior of imperfect cylindrical shells subject to a uniformly distributed axial compression applied on two symmetrically located zones on one boundary. This loading arrangement is referred to here as "partial axial compression". Following the Eurocode (ENV 1993-1-6, 1999) formulation for describing the separate effects of imperfection sensitivity and plasticity, this study describes the nonlinear and imperfect buckling loads in terms of the linear bifurcation load $q_{\mathrm{cr}}^{\mathrm{L}}$ for the same loading condition.

2. Aspects of finite element analysis

2.1. Geometry, loading and material properties

All the numerical analyses were conducted using the ABAQUS program (Hibbit et al., 1998) on a single shell global geometry defined by $L/R = 3$, $R/t = 500$ ($t = 1$ mm) (Fig. 1). The main parameters considered in the study included the size of the loaded zone (subtended angle of the partial load), and the form, amplitude and position of geometric imperfections. The partial axial compression consists of two uniformly distributed loads q on the top edge of the shell, symmetrically placed and each spanning over a circumferential angle of $2\theta_n$. A cylindrical co-ordinate system (Fig. 1) was used, with the origin located at the base.

The geometric imperfections were all represented by a complete definition of the imperfect shape, using doubly curved elements to capture local shell forms and ensure geometric and deformation compatibility between elements. Appropriate care was taken with mesh refinement where the imperfect geometry led to high local curvatures. The shell was assumed to be stress free in its imperfect geometry, since studies of consistent residual stresses in similar shells (Rotter, 1996; Holst et al., 2000) suggest that residual stresses are both small and usually beneficial to the shell buckling strength under axial compression.

Both shell ends were simply supported S3 (Yamaki, 1984). All translational degrees of freedom w, v and u (DoFs 1, 2 and 3 in Fig. 1) were restrained on the bottom edge, while the axial displacement u (DoF 3) was left free on the top edge. Based on the conclusions reached in Song (2002), on both edges the rotations

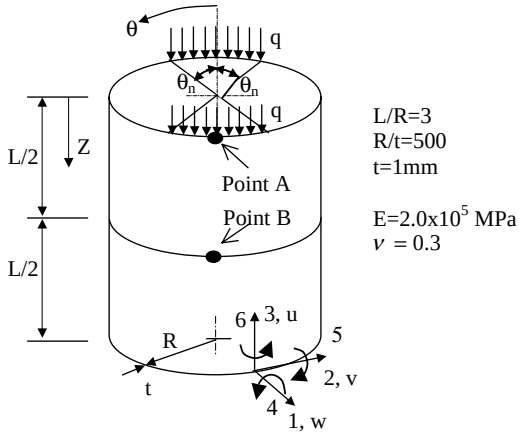

Fig. 1. Cylinder subject to partial axial compression.

about the meridional and normal axes were restrained to produce classical S3 boundaries and to prevent the occurrence of spurious modes. The existence of two axes of symmetry made it possible for a quarter model to be used, although care needs to be exercised in using such quarter models, because the symmetry exploited may be destroyed by a mode change during the deformation process as shown in Teng and Song (2001). Numerical models in which excessive symmetry is imposed are subjected to additional artificial restraints and their buckling loads are overestimated. Teng and Song (2001) also showed that a half-structure model is generally as satisfactory as a whole-structure model for modes that involve only part of the circumference, except when torsional deformations occur. Thus, provided mode changes do not occur, symmetry conditions can be utilised with full confidence to save computing time. In the present investigation, a half-structure model was adopted instead of a whole-structure model for most cases. Full exploitation of symmetry was reserved for loads with small subtended angles (e.g. $2\theta_n = 2°, 5°$); the validity was ensured by comparing these results with those of half-structure models for selected cases.

The material was assumed to be isotropic and linear elastic, with a Young's modulus $E = 2.0 \times 10^5$ MPa and a Poisson's ratio $v = 0.3$, which are typical values for steel.

2.2. Analysis types used

The study is chiefly concerned to establish the strength of imperfect elastic cylinders subject to partial axial compression. Following the description of the Eurocode (ENV 1993-1-6, 1999), linear eigenvalue buckling (here termed linear bifurcation) analyses (LBA) provide the reference buckling loads for all conditions, as well as candidate mode shapes for geometric imperfections. Geometrically nonlinear elastic analyses of the perfect shell (GNA) provide limit point loads for the perfect structure, which indicate the importance of geometric nonlinearity in each loading case, and provide additional candidate imperfection forms. During a GNA analysis, the possibility of bifurcation needs to be checked at each load step to determine the nonlinear bifurcation load and the corresponding bifurcation mode, which is another candidate imperfection form. The chief results of this paper are, however, derived using geometrically nonlinear elastic analyses with explicit representation of geometric imperfections (GNIA) to obtain bifurcation and limit load points for the imperfect structure.

The nonlinear load–deflection path was followed using the arc length method (Riks, 1979), and the determinant of the stiffness matrix was checked at each iterative step to determine if one or more negative eigenvalues had appeared. The appearance of a negative eigenvalue indicates that a bifurcation point on the

load–deflection path has been passed. Where this situation arose, a subsequent nonlinear analysis with eigenvalue analysis at a number of adjacent load levels was conducted to accurately determine the bifurcation load. The buckling loads reported in this paper correspond either to bifurcation loads identified by eigenvalue analyses or to limit point peaks on the geometrically nonlinear path. It should be noted that, of all the cases investigated in this study, nonlinear bifurcation was only detected in some of the shells with a weld depression imperfection.

2.3. Shell elements

Alternative shell elements suitable for a general nonlinear load–deflection analysis in the ABAQUS program were evaluated by Song (2002). The 8-node and 9-node isoparametric thin shell elements with reduced integration, S8R5 and S9R5 (each with 5 DoFs per node), are suitable for nonlinear buckling analyses of thin shells due to their robustness and their quadratic representation of the curved surface. Whilst these two elements generally perform similarly, the S8R5 element is more economic than S9R5. On the other hand, the lack of an interior node in S8R5 makes this element more sensitive to element shape distortion (e.g. MacNeal, 1994). For circular cylindrical shells, there is no good reason not to use rectangular elements, so element shape sensitivity is not an important issue. The S8R5 8-noded isoparametric shell element with reduced integration was therefore used throughout this study.

2.4. Mesh convergence study

2.4.1. General

Several mesh convergence studies were conducted first. A good approach for such studies is to adopt a mesh which provides almost identical results to those from a further refined mesh (e.g. the buckling load is changed by less than 1% as a result of halving the mesh size). This study followed this approach: the aim of this paper is to undertake parametric studies of the buckling and post-buckling behavior of cylindrical shells with and without imperfections, so the mesh convergence study aimed to find meshes that predict both the buckling and the post-buckling behavior accurately, without excessive computing effort. Appropriate attention was paid to mesh refinement in the imperfection zones (especially weld depressions), since careful definition of the doubly curved geometry of a local imperfection is essential to an accurate determination of the buckling strengths of locally imperfect shells (Rotter and Teng, 1989; Teng and Rotter, 1992).

For shell buckling and post-buckling analysis, discretisation into finite elements is best discussed in terms of the number of elements or nodes per half-wavelength of the relevant bending or buckling deformations (these also relate to imperfection geometries). In the present study, the half-wavelength λ_{cl} of the axisymmetric buckling mode (Yamaki, 1984)

$$\lambda_{cl} \approx 1.728\sqrt{Rt} \tag{1}$$

was used as a yardstick because mesh sizes must relate to buckling modes. This length ($=38.64t$ in all the calculations performed in this study) is simply referred to as the half-wavelength, unless there is a need to differentiate it from the linear elastic bending half-wavelength λ_b, given by:

$$\lambda_b = \sqrt{2}\lambda_{cl} \approx 2.444\sqrt{Rt} \tag{2}$$

In Teng and Song (2001), it was shown that the deformation path of a shell calculated from a nonlinear finite element analysis using the arc-length method (Riks, 1979) can be sensitive to the maximum arc-length increment allowed for each loading step. Results obtained with the maximum arc-length increment $\Delta l_{max} = 0.1$ are discussed here. To save computational time, a mesh convergence study was performed for each load

angle to find the most economic model. The results of mesh convergence studies for two representative load angles are given here.

2.4.2. Mesh convergence for a narrow partial load ($2\theta_n = 5°$)

Finite element predictions were obtained using three different meshes for the problem shown in Fig. 1 with the partial loading acting over an angle $2\theta_n = 5°$ for each loading zone. The results are shown in Table 1. The meshes are described in terms of the circumferential nodal spacing in degrees and the meridional nodal spacing as a proportion of the half-wavelength λ_{cl}. For the shells studied here, the classical buckling half-wavelength λ_{cl} corresponds to a circumferential angle of 4.428. Thus, Mesh C has $0.125°/0.0833\lambda_{cl}$ denoting a circumferential nodal spacing of 0.125° and a meridional nodal spacing of $\lambda_{cl}/12$.

The linear bifurcation buckling loads q_{cr}^{L} and the limit point loads on the geometrically nonlinear path q_{max} of the perfect shell are listed in Table 1. The values change less than 1% on mesh refinement, suggesting that even the coarsest Mesh A is adequate. However, the calculated post-buckling path (Fig. 2) is not followed by Mesh A, indicating that it is unsatisfactory. In Fig. 2, the abscissa is the axial displacement u at the centre of the load (Point A shown in Fig. 1), divided by the shell thickness, while the ordinate is the local value of the partial distributed axial load q divided by the linear bifurcation buckling load (q_{cr}^{L}). The load–deflection paths predicted by Meshes B and C are very close to each other, but the analysis using the coarse Mesh A did not find the post-buckling path, but descended back down the pre-buckling path. Mesh D was a further refinement and predicted practically the same buckling load and post-buckling path as those from Mesh C. The inability of the coarse Mesh A to capture the post-buckling path may be due to its coarseness, though the limitation of the maximum arc-length increment may also be a factor.

2.4.3. Mesh convergence for a wide partial load ($2\theta_n = 30°$)

A mesh convergence study for the load angle $2\theta_n = 30°$ is described next. Four meshes of increasing density were employed, leading to the predictions listed in Table 2, where all four meshes can be seen to

Table 1
Mesh convergence study for $2\theta_n = 5°$

Mesh name	Nodal spacing circ./merid.	Nodes per half-wavelength	q_{cr}^{L} (N/mm)	q_{max}/q_{cr}^{L}
A	$0.3125°/0.125\lambda_{cl}$	14/8	413.27	0.753
B	$0.25°/0.125\lambda_{cl}$	18/8	413.22	0.753
C	$0.125°/0.0833\lambda_{cl}$	35/12	413.20	0.752
D	$0.0833°/0.0625\lambda_{cl}$	53/16	413.10	0.750

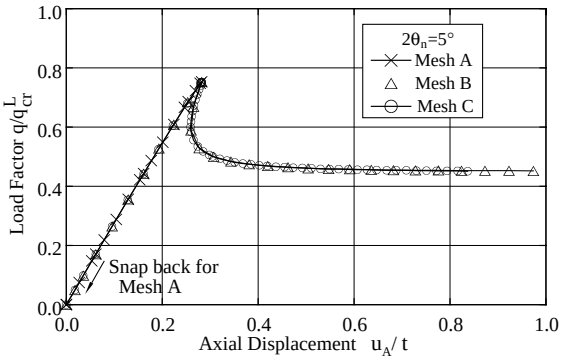

Fig. 2. Load–deflection curves from GNA analyses of the perfect cylinder under partial axial compression with $2\theta_n = 5°$ using different meshes.

have predicted essentially the same linear bifurcation and limit point buckling loads. The post-buckling paths are also close to each other, as shown in Fig. 3. In Mesh E, the number of nodes per half-wavelength in each direction was fewer than 4, and even Mesh H involved fewer nodes overall than those used for $2\theta_n = 5°$. The agreement between the results predicted by all 4 meshes indicates that the coarse Meshes E and F can be used with confidence in nonlinear analyses for this load angle, but it should be noted that these results were obtained with the maximum arc-length increment limited to $\Delta l_{\max} = 0.1$.

2.4.4. Other cases

Similar mesh convergence studies were conducted for other load angles. Table 3 lists some of the final meshes that are used later in the imperfection-sensitivity studies of all imperfection modes except weld depressions.

Two meshes were devised for $2\theta_n = 90°$ (Table 4): one with uniform nodal spacing down the meridian (Mesh I), the other with non-uniform spacing (Mesh J), with the first $10.35\lambda_{cl}$ of shell just beneath the load uniformly discretised, but larger and non-uniform divisions for the remainder. Both meshes led to the same buckling loads and load paths (Fig. 4). It should be noted that two sets of load–displacement curves are shown in Fig. 4, one with the abscissa being the radial displacement w of Point B (Fig. 1) located at the mid-height of the shell divided by the shell thickness, and the other with the abscissa being the same as that used

Table 2
Mesh convergence study for $2\theta_n = 30°$

Mesh name	Nodal spacing circ./merid.	Nodes per half-wavelength	q_{cr}^{L} (N/mm)	$q_{\max}/q_{cr}^{L}$
E	$1.25°/0.259\lambda_{cl}$	3.5/3.9	250.75	0.787
F	$0.75°/0.194\lambda_{cl}$	5.9/5.2	250.38	0.787
G	$0.50°/0.129\lambda_{cl}$	8.9/7.7	250.15	0.788
H	$0.33°/0.0776\lambda_{cl}$	13.3/12.9	250.07	0.790

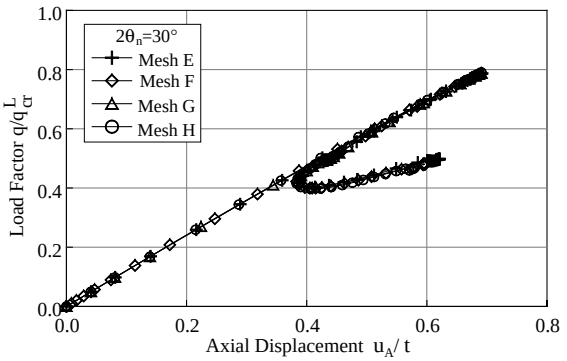

Fig. 3. Load–deflection curves from GNA analyses of the perfect cylinder under partial axial compression with $2\theta_n = 30°$ using different meshes.

Table 3
Final meshes used in the imperfection sensitivity study

Load angle $2\theta_n$	30°	60°	90°	150°
Mesh	$0.75°/0.194\lambda_{cl}$	$1.5°/0.259\ \lambda_{cl}$	$1.5°/0.388\lambda_{cl}$	$1.5°/0.388\lambda_{cl}$

Table 4
Mesh convergence study for $2\theta_n = 90°$

Mesh name	Nodal spacing circ./merid.	q_{cr}^{L} (N/mm)	q_{max}/q_{cr}^{L}
I	1.5°/0.388 λ_{cl}	219.5	0.749
J	0.9375°/0.259 λ_{cl}	219.0	0.751

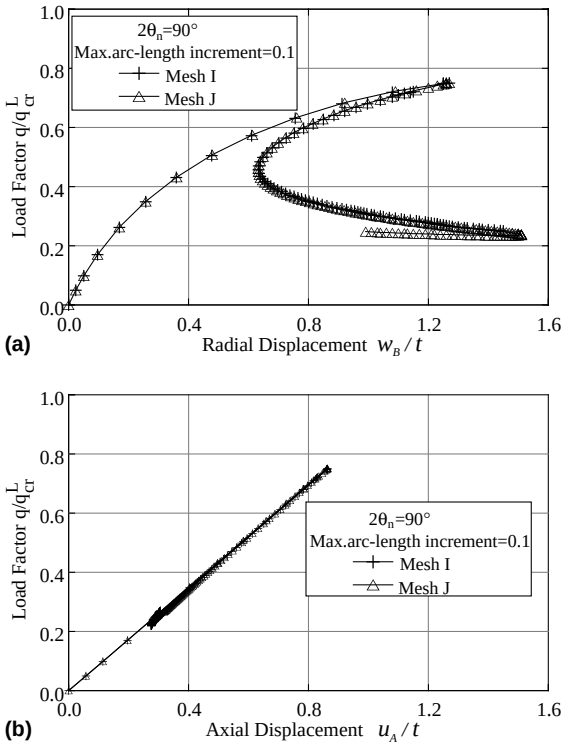

Fig. 4. Load–deflection curves from GNA analyses of the perfect cylinder under partial axial compression with $2\theta_n = 90°$ using different meshes.

in Figs. 2 and 3 for the narrower loads. Fig. 4a is shown here to better distinguish the pre-buckling path from the post-buckling path, as in Fig. 4b, the two can hardly be separated.

The mesh convergence studies described above were conducted with the maximum arc-length increment limited to $\Delta l_{max} = 0.1$. During this convergence study, it was recognized that this increment may play a significant and interactive role with the fineness of the mesh in determining whether the post-buckling path is properly captured. Further information on this subject may be read in Song (2002).

When a weld depression was considered, the mesh was carefully refined near the weld depression. For a weld depression centered at a distance of one meridional bending half wavelength from the loaded edge of the shell, a graded mesh with 24 nodes for the first two meridional bending half wavelengths from the loaded edge was used. Comparisons of finite element GNA results using such a mesh and those from a mesh with 32 nodes for the first two bending half wavelengths showed almost no difference, with the peak loads differing by less than 1%. For other cases with a weld depression, meshes of similar refinement were used.

3. Buckling of perfect shells under partial axial compression

To obtain a comprehensive and compatible set of reference buckling strengths in terms of the European Standard for shell design (ENV 1993-1-6, 1999), calculations were first carried out to determine the linear elastic bifurcation loads and the associated bifurcation modes of perfect shells subject to partial axial compression. The load angle was varied from $2\theta_n = 2°$ to $2\theta_n = 180°$, the latter corresponding to uniform axial compression. The results are summarized in Fig. 5, where the buckling load per unit circumference on the loaded zone of the boundary q_{cr} is divided by the classical elastic critical load per unit circumference for uniform compression q_{cl}

$$q_{cl} = 0.605E\frac{t^2}{R} \tag{3}$$

in which t is the thickness of the shell, R is its radius and E is Young's modulus.

For very localised compression (small θ_n), the applied stress required to cause buckling is naturally very high. It might have been expected that the buckling stress would reduce steadily as the load angle increases, tending to the value for uniform compression as that condition is approached ($2\theta_n = 180°$). However, the real behavior is a little more complex, with the buckling load intensity falling below that for uniform compression for intermediate values of the load angle (Fig. 5). The reason can be found by examining the linear bifurcation modes (Fig. 6) for $2\theta_n = 2°$, 5°, 10°, 30°, 90° and 150°. At small load angles, the buckles occur locally beneath the center of the load, but as the load angle increases, the buckles extend over the entire shell height. A similar division into two different modes was found by Cai et al. (2002, 2003).

The buckling modes for $2\theta_n = 90°$ and 150° (Fig. 6) suggest that the shear stress may become important. The distributions of meridional membrane stress and membrane shear stress around the circumference at a distance $Z = 10\lambda_{cl}$ away from the loaded edge are shown in Fig. 7 at the instant of linear bifurcation buckling. The stress discontinuity at the edge of the partial load ($\theta = \theta_n$) causes a membrane displacement discontinuity, which leads to high shear stresses in the shell. Even though the shear stress is much smaller than the axial stress, it is influential: the peak value τ_{max} may be compared with the classical uniform torsional buckling stress τ_{cl} for a simply supported cylinder (Timoshenko and Gere, 1963), which is closely approximated by

$$\tau_{cl} = 0.75E\left(\frac{R}{L}\right)^{1/2}\left(\frac{t}{R}\right)^{5/4} \tag{4}$$

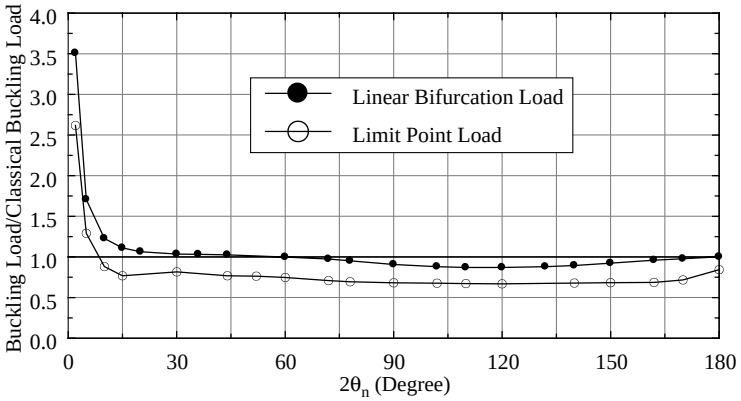

Fig. 5. Linear and nonlinear bifurcation loads for perfect cylinders under partial axial compression over different load angles.

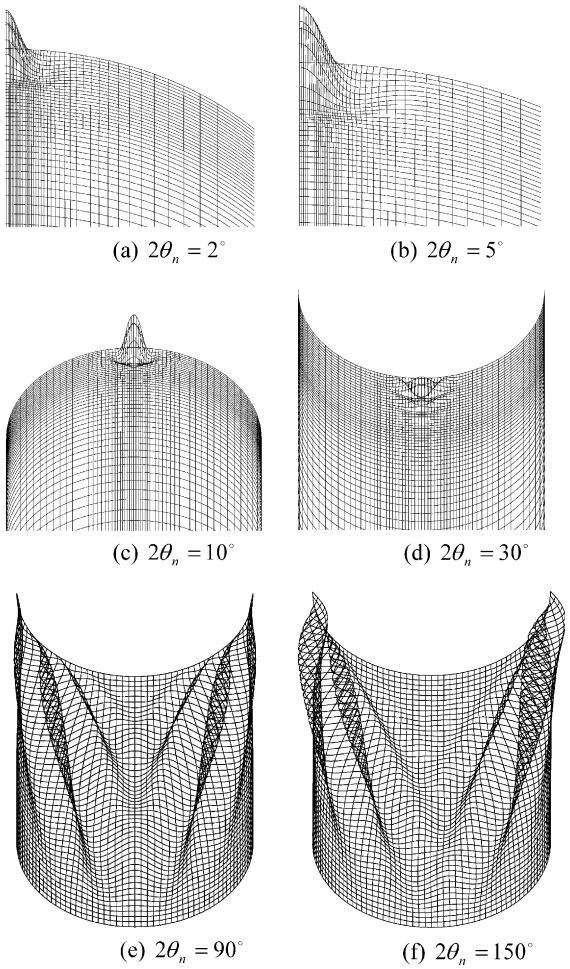

Fig. 6. Linear bifurcation modes of the perfect cylinder.

If the relevant length L is taken as the full shell length here, the maximum shear stress τ_{max} in Fig. 7 is $0.94\tau_{cl}$, with the shear increasing towards the loaded edge. Thus, for a wide partial load, the buckling mode (Fig. 6) is strongly affected by the induced shear stress associated with the edge of the load. This phenomenon was also found by Cai et al. (2002, 2003).

For these locally loaded shells, no bifurcation was detected during any of the GNA analyses which led to the determination of the limit point buckling loads only. The effect of geometric nonlinearity on the buckling load (the ratio of the limit point buckling load to the linear bifurcation load) is shown in Fig. 8. The shell under partial axial compression is quite sensitive to the effect of geometric nonlinearity (typically a 25% reduction), which compares with the lesser effect on a uniformly compressed shell (15% here).

Due to the absence of a bifurcation point along the nonlinear load–deformation path, the limit point load was also confirmed as the buckling load by eigenvalue analyses based on the deformed and loaded structure. Such eigenvalue analyses produced eigenmodes which are shown in Fig. 9. It should be noted that these eigenmodes are not bifurcation modes as they are in fact in the incremental mode of the deformation of the shell at the limit point load. These modes are referred to herein as nonlinear buckling modes and

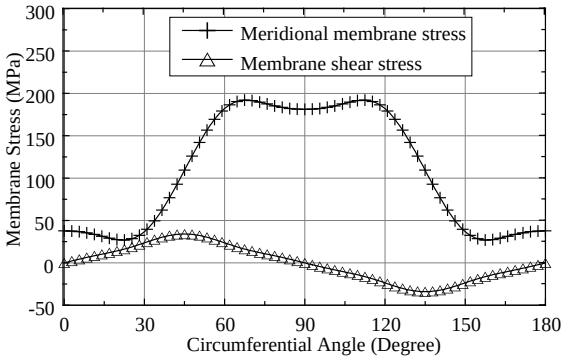

Fig. 7. Membrane stress distributions around the circumference in the perfect cylinder under partial axial compression with $2\theta_n = 90°$.

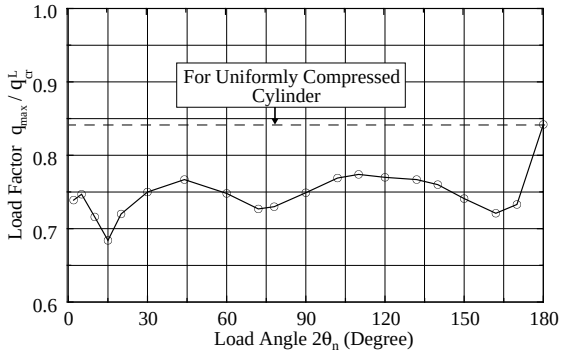

Fig. 8. Ratio of limit point load to linear bifurcation load, indicating the effect of geometric nonlinearity.

taken as candidate imperfection forms in place of nonlinear bifurcation modes from such eigenvalue analyses when a bifurcation point exists prior to the limit point. The term "nonlinear buckling modes" is also used to refer to both types of modes in discussions where a differentiation of the two is unnecessary. It is worth noting that these eigenmodes are sometimes quite different from their linear bifurcation counterparts (compare Figs. 6 and 9) (e.g. $2\theta_n = 30°, 90°, 150°$).

4. Imperfection forms

4.1. Introduction

The load-carrying capacity of an axially compressed cylindrical shell is strongly influenced by the distribution and amplitude of geometric imperfections in the shell. The alternative choices made by different researchers who were looking for practical but severe forms of imperfection for axially compressed cylinders were discussed by Rotter (2004). Esslinger and Geier (1972) and Yamaki (1984) explored many different concepts for imperfection forms, and their ideas were used by Guggenberger (1992) and by Greiner and Derler (1995) and Schneider et al. (2001) in studies of local supports and wind loading. However, all these analyses showed that the worst imperfection form depends on the shell geometry and loading. General conclusions could not be obtained from their analyses.

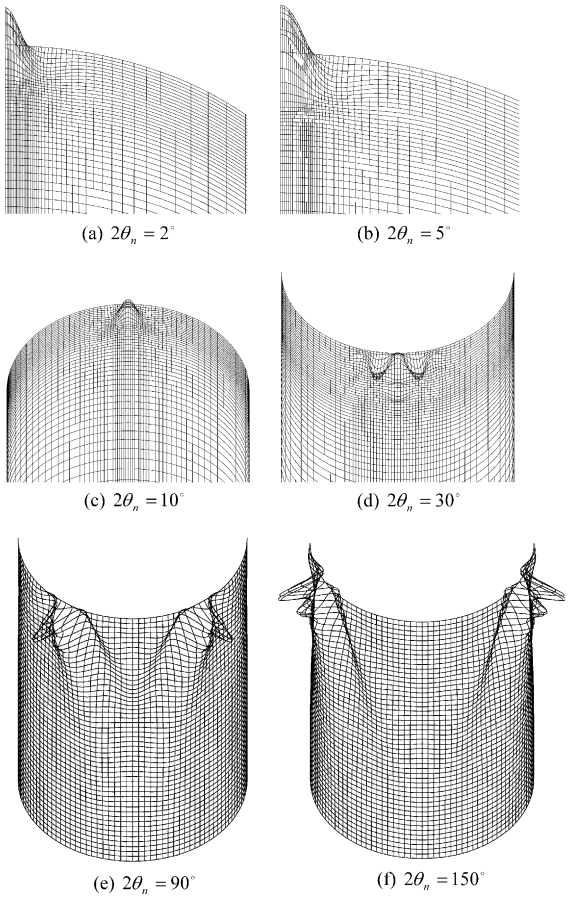

Fig. 9. Nonlinear buckling modes of the perfect cylinder.

In this study, four types of imperfection form, drawn from ideas in these studies, were considered: the linear bifurcation mode (LBM), the nonlinear buckling mode (NBM), post-buckling deformed shapes (PDS), and local weld depressions (WD).

4.2. Linear bifurcation buckling modes

The linear bifurcation mode of the perfect shell has long been used (Koiter, 1945, 1963; Yamaki, 1984; Speicher and Saal, 1991) as an equivalent imperfection form, because it is easily obtainable and generally gives a relatively severe form of imperfection (ENV 1993-1-6, 1999).

4.3. Nonlinear buckling modes

The nonlinear buckling mode, either the incremental mode at the limit point load or the nonlinear bifurcation mode, may be quite different from the linear bifurcation mode. It thus provides another equivalent imperfection form. These modes are shown in Fig. 9 for a range of different load angles θ_n.

4.4. Post-buckling deformed shapes

Alternative forms taken from the post-buckling path for the perfect shell have been employed by some researchers (Esslinger and Geier, 1972; Guggenberger et al., 2000; Schneider et al., 2001). Imperfections based on post-buckling deformed shapes may have a more severe effect than other imperfection forms, such as that taken from the linear bifurcation mode. However, since geometric nonlinearity can cause the buckling phenomenon to disappear in a perfect elastic shell, even though buckling will occur in the imperfect elastic–plastic shell, both the nonlinear buckling mode and the post-buckling mode lack the generality of the linear buckling mode (Rotter, 2002) and are therefore less satisfactory as a general concept to be applied to all load cases on all shell geometries.

Further, it is difficult to define the post-buckling deformed shape in a unique and repeatable manner because its form changes progressively (Yamaki, 1984; Riks et al., 1996; Rotter, 2004). Whilst it might be desirable to investigate several alternative post-buckling deformed shapes for the imperfection, the choice was restricted here to three patterns for practical reasons. All three were obtained from the falling post-buckling path after the limit point. Patterns derived from modes deep in the post-buckling path were not considered, as they are difficult and time-consuming to obtain and are often not unique (sensitive to solution process, mesh refinement and element formulation).

The post-buckling deformed shapes were obtained from the following points on the post-buckling path: immediately after the limit point, at the lowest load and between these two extreme cases, as shown schematically in Fig. 10. These three points were designated as 'Max', 'Min' and 'Mid' respectively. The 'Max' and 'Min' points are easily identified, but the 'Mid' point depends a little on the form of the post-buckling curve, which itself depends strongly on which displacement variable is plotted. For simplicity, the 'Mid' point was chosen to be at a load half way between those at the limit point and the minimum post-buckling load. In the actual implementation, the load of the "Mid" point was only approximately half way between the other two loads, as loading increments were dictated by the solution process of ABAQUS and displacements were output at selected load steps to save disk space. Any difference caused by this approximation is small.

The imperfection amplitude δ is here defined as the maximum departure of the imperfect shell in the direction normal to the perfect geometry. Thus, to define an imperfection with an amplitude of δ in the shape of the post-buckling pattern at a selected point on the load path, the largest radial displacement $w_{\max}$ must be found and a scaling factor k found as the ratio of the chosen imperfection amplitude δ to $w_{\max}$. The entire post-buckling deformed shape is then scaled by k. This makes the procedure rather complicated, because every member of a parametric study has a different imperfection mode and each must be processed in this manner: bifurcation buckling mode imperfections are easier to implement. Without an automated routine to perform the task, post-buckling modes become very tedious to use. A further disadvantage stems from the sensitivity of the post-buckling path to many factors associated with the calculation process, so these imperfections should not be demanded without careful thought.

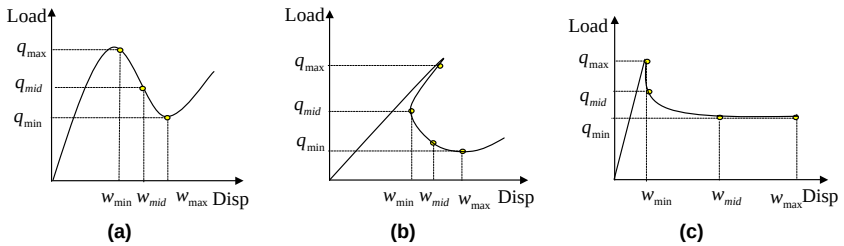

Fig. 10. Points on the perfect shell post-buckling path used to develop imperfection forms.

It should be noted that the post-buckling deformed shape contains components of both the pre-buckling and buckling deformations. Thus, the deformed shape termed 'Max' here may be dominated by the pre-buckling deformations (which are not axisymmetric), with only a small component of the nonlinear buckling mode added. It is thus likely to produce a rather different geometric imperfection from the linear bifurcation mode or the nonlinear buckling mode.

4.5. Weld depressions

The first modern study of imperfections (Koiter, 1945) adopted the axisymmetric linear bifurcation mode and showed the high sensitivity to imperfection amplitude. This continuous sinusoidal imperfection was explored further by Tennyson and Muggeridge (1969), who found that the critical imperfection wavelength varies with the imperfection amplitude. For very small amplitudes, they confirmed Koiter's deduction that the critical half-wavelength approaches the classical axisymmetric buckling mode half-wavelength λ_{cl}, but they found that the critical wavelength increases as the imperfection amplitude increases, approaching the linear meridional bending half-wavelength λ_b (Eq. (2)) as the amplitude δ approaches twice the shell thickness. However, this was based on an asymptotic analysis that is accurate only for small imperfections.

Imperfections in the form of linear bifurcation modes, nonlinear buckling modes and post-buckling deformed shapes are all idealised forms that are generally not found with significant components in real shell structures. Imperfections in real structures take different forms, the simplest and most easily recognisable of which is probably the axisymmetric weld depression (Rotter and Teng, 1989). Teng and Rotter (1992) and Rotter (1997) studied this form with a rigorous nonlinear analysis and found that the critical wavelength for an amplitude equal to the thickness is already 25% longer than the linear bending wavelength. Higher amplitudes lead to even longer critical wavelengths (Rotter, 2004). Berry et al. (2000) measured the form of the weld imperfection in their fabricated specimens and found that the actual half-wavelength, with 90% confidence limits was given by

$$\lambda = (0.97 \pm 0.02)\lambda_b \tag{5}$$

which indicates that real wavelengths are close to those originally adopted by Rotter and Teng (1989). The above conclusions from existing studies on uniformly compressed shells give a clear description of conditions for uniform compression, but the same conclusions cannot be applied to non-uniform axial loads, since the buckling modes are quite different. In particular, determination of whether a weld depression is a severe form of imperfection for local compression needs investigation. Under partial axial compression, the buckling load depends on the imperfection amplitude and its wavelength, but also on its distance from an end boundary condition.

The shape of the typical weld depression and its effect on the buckling strength under uniform axial compression has been studied using both theoretical and experimental methods by many authors (Rotter and Teng, 1989; Rotter, 1996, 1997; Ding et al., 1996; Berry et al., 2000; Pircher and Bridge, 2001a,b; Pircher et al., 2001). Rotter and Teng (1989) proposed two limiting cases for the geometry, based on linear shell bending theory: the weld was either rotationally stiff during shrinkage (Type A) or rotationally free during shrinkage (Type B). Between these two extremes lie a set of alternative forms that were explored by Berry et al. (2000) and Pircher et al. (2001). The expression for the Type A weld depression (Rotter and Teng, 1989) was formulated using the above assumption and elastic shell bending theory for a long cylinder and is given by

$$w = \delta\, e^{-(\pi x/\lambda)}\left(\cos\frac{\pi x}{\lambda} + \sin\frac{\pi x}{\lambda}\right) \tag{6}$$

The expression for a Type B depression, based on zero rotational stiffness during shrinkage is:

$$w = \delta \mathrm{e}^{-(\pi x/\lambda)}\left(\cos\frac{\pi x}{\lambda}\right) \tag{7}$$

Since the weld has a certain stiffness and can bear some moment during the later stages of cooling, real welds lie between these two extremes. Taking this stiffness into account, the weld depression can be expressed as (Berry et al., 2000):

$$w = \delta \mathrm{e}^{-(\pi x/\lambda)}\left(\cos\frac{\pi x}{\lambda} + k\sin\frac{\pi x}{\lambda}\right) \tag{8}$$

where k is a parameter describing the degree of rotational continuity at the weld, with $k = 1$ and $k = 0$ corresponding to Types A and B respectively. According to the above derivation, the half-wavelength of the bending deformation λ should be the linear bending value λ_b, but the above studies showed that a secure conservative choice of this parameter depends on the amplitude of the imperfection δ. Pircher et al. (2001) studied the measurements made by Rotter et al. (1992) and Ding et al. (1996) on a full scale silo and found that the measured imperfections and wavelengths differed a little from the simple Type A model. However, in view of the limited number of silo measurements available, the conservatism of the choice of Rotter and Teng's Type A depression, and its extensive use in other theoretical studies, this form (Eq. (4)) was used here as a moderately accurate but conservative representation.

A weld depression imperfection can be placed anywhere throughout the height of a shell, so before any general conclusions can be obtained, information concerning the effect of weld depression location is required. Under uniform compression, the location is unimportant unless adjacent depressions cause interactions (Rotter, 1996), or the weld is so close to an end boundary that the boundary conditions provide restraint, but where a varying stress field is involved, the location can strongly affect the strength. This is explored in Section 5.

5. Buckling strength of imperfect cylinders

5.1. Introduction

The Eurocode for shell structures (ENV 1993-1-6, 1999), defines three different amplitudes of geometric imperfection for a shell of given geometry, according to the fabrication quality class. The specified amplitude for fabrication tolerances and hand calculations (Sections 8.4 and Annex D) is different from the value given for nonlinear finite element analysis (Section 8.8.2). For nonlinear analysis of the present cylinder, the lowest quality class specification leads to an imperfection amplitude of about $2.5t$, so values up to $2.5t$ must be considered for this shell. Larger amplitude imperfections were also considered here for the sake of completeness. All the analyses were conducted using a GNIA analysis. The following sections review issues associated with each type of imperfection before finally presenting comparisons between the lowest strength found for each type.

5.2. Shells with linear bifurcation mode (LBM) imperfections

Imperfections in the form of the linear bifurcation mode were studied first. Typical load–deflection curves for imperfect shells under partial axial compression are shown in Fig. 11 ($2\theta_n = 30°$). For clarity, the behavior at small imperfection amplitudes is shown in Fig. 11(a), while that at larger imperfection amplitudes is in Fig. 11(b). The curves in Fig. 11(a) indicate that the shell buckles dynamically when δ/t is small. As the imperfection amplitude increases, the limit point load falls to a minimum of $q/q_{cr}^{L} = 0.235$ at about $\delta/t = 6$, after which any further increase in the geometric imperfection amplitude has a strengthening

effect. However, the post-buckling path is unstable for all amplitudes. The pre-buckling path becomes very nonlinear for large imperfection amplitudes. It may be noted that the Eurocode "lowest quality" fabrication produces a strength of $q/q_{cr}^{L} = 0.34$ that is far (in this case 45%) above the minimum, so design philosophies based on lower bound strengths (e.g. Ellinas and Croll, 1986) can be very uneconomic. Further results from LBM imperfections are given below.

5.3. Shells with nonlinear buckling mode (NBM) imperfections

In all analyses of imperfect shells, the imperfect shape was obtained by adding an imperfection to the perfect shell. An eigenmode is, by definition, an incremental displacement whose direction is undefined, so when such imperfections are used, the maximum deviation in the resulting imperfect shell may be either inward or outward. The difference in buckling strength between inward and outward imperfections for both LBM and NBM imperfections is shown in Fig. 12. It is evident that inward dents are always more detrimental than outward bulges, except for the special case of LBM imperfections with $2\theta_n = 150°$, when the difference is marginal. This extends the conclusion reached by Teng and Rotter (1992) concerning uniform compression to more general load cases. It may also be seen in Fig. 12 that LBM and NBM imperfections sometimes produce the same form of imperfection sensitivity curve, and sometimes produce quite different shapes, depending on the load angle. Further comparisons are given below.

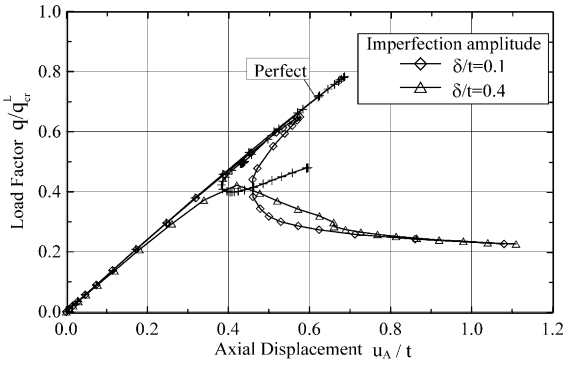

(a) Small amplitude imperfections

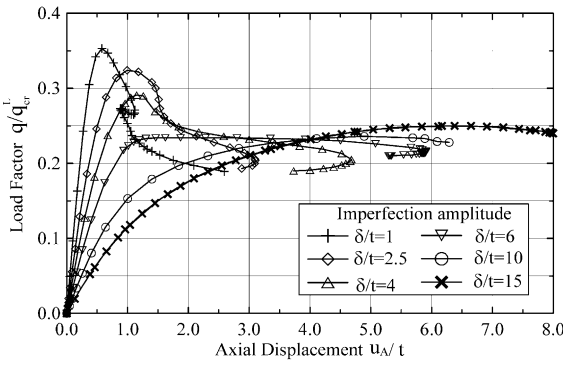

(b) Large amplitude imperfections

Fig. 11. Load–deflection curves of shells with LBM imperfections for $2\theta_n = 30°$.

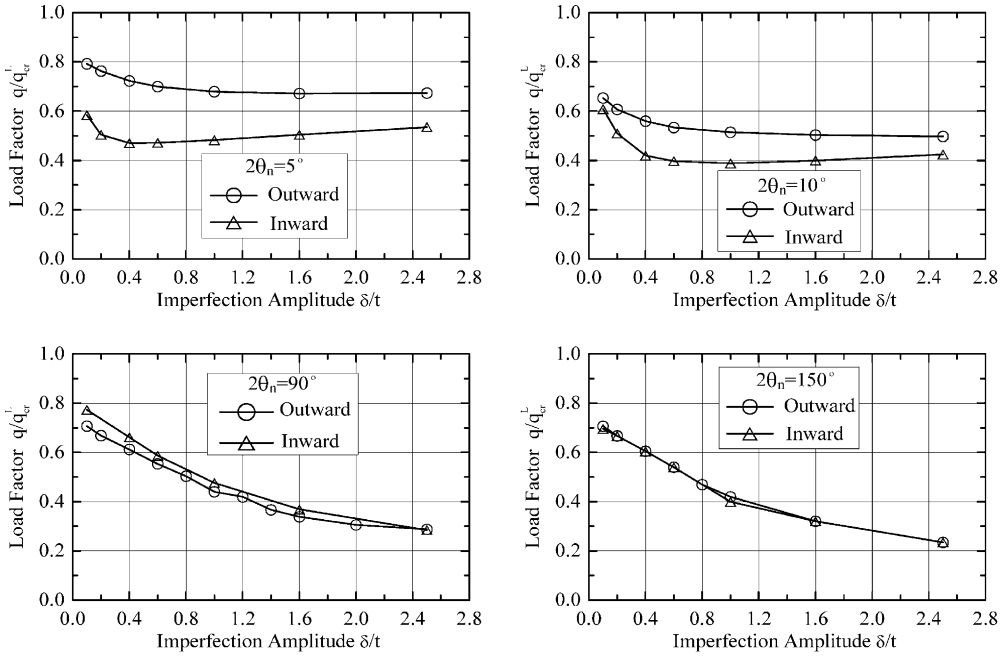

(a) LBM imperfections

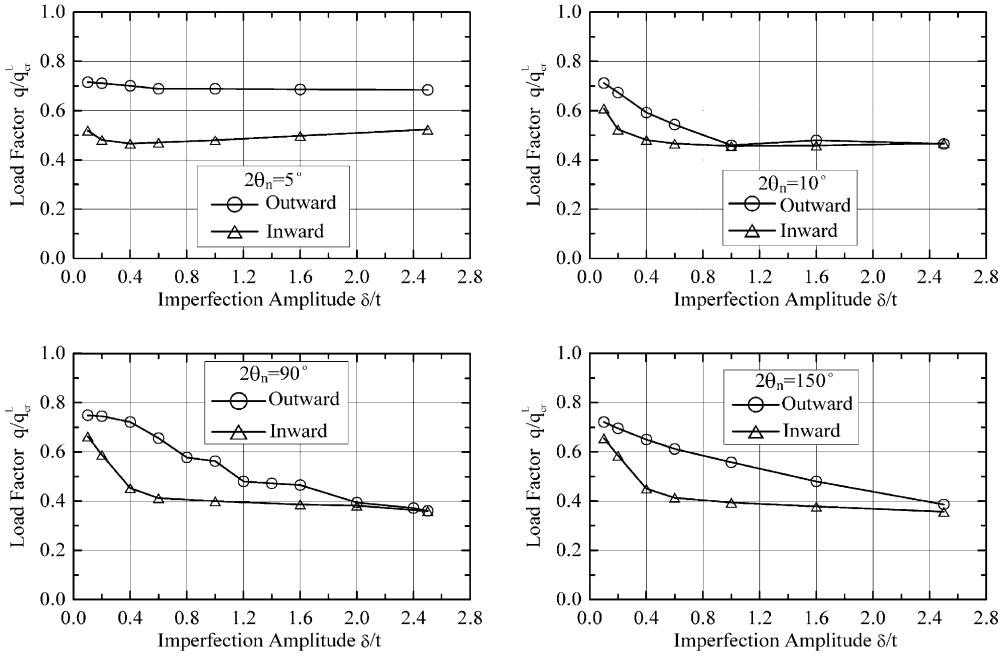

(b) NBM imperfections

Fig. 12. Effect of inward and outward imperfections on the buckling load.

5.4. Shells with post-buckling deformed shape (PDS) imperfections

In Section 4, alternative points are defined that might be used to obtain imperfection forms from the nonlinear perfect shell post-buckling path, which are identified as the 'Max', 'Mid' and 'Min' points. As an example, the imperfection sensitivity curves for a partial load angle of $2\theta_n = 90°$ are shown in Fig. 13. For this case, the 'Mid' imperfection causes the greatest strength loss at small amplitudes, but the 'Min' imperfection becomes critical at larger amplitudes. It might also be supposed that the 'Max' imperfection would be critical for very small imperfections. The lower bound on these different curves is also marked with a thick line to indicate how these results will be used in the later comparison. It is clear that where post-buckling deformed shapes are used as imperfection forms, there is no simple answer to the point on the load–deflection curve that should be used to obtain the 'worst' shape. Further results from PDS imperfections are given below.

5.5. Weld depression imperfections

5.5.1. Influence of weld depression position

As noted earlier, when the weld depression imperfection is used in a varying stress field (She and Rotter, 1993), both the location and the wavelength of the imperfection must be adjusted to identify the worst case. Following the discussion above, the reference half-wavelength of the depression was taken as λ_b. The location is defined here in terms of the distance d of the centre of a Type A weld depression from the loaded edge of the shell (Fig. 14). For most of the imperfections studied here, the distance d is so large that the load eccentricity δ_e is negligibly small.

Since the stress field in the shell varies as the load disperses into it, it might be supposed that the lowest buckling load would occur if the weld depression is placed at the location where the meridional membrane compressive stress is maximum. The distribution of this stress from an LA analysis of the perfect shell is shown in Fig. 15 for the partial load $2\theta_n = 5°$ at the load intensity $q = 100$ N/mm. The maximum stress always occurs at the loaded edge (Fig. 15). Profiles of the meridional membrane stress down the meridian passing through Point A (Fig. 1) are shown in Fig. 16 for two partial load angles ($2\theta_n = 5°$ and 90°). For both cases, the maximum occurs at the loaded edge. For the small angle $2\theta_n = 5°$, the stress attenuates quickly down the meridian, but for the wider $2\theta_n = 90°$, the attenuation is slow. Buckling is stimulated by high stresses, but stabilised by the proximity of a boundary restraint: the critical location depends on the balance between these two effects. The LBM and NBM buckling modes should provide a good guide to this worst position. The displacement distributions down the meridian of both the linear bifurcation mode and

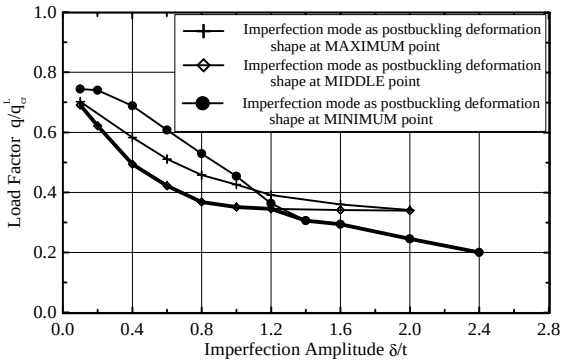

Fig. 13. Effect of PDS imperfections on the buckling load for $2\theta_n = 90°$.

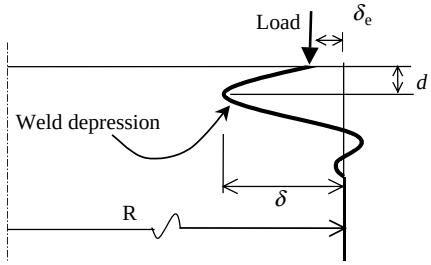

Fig. 14. Weld depression shape near the loaded edge of the cylinder.

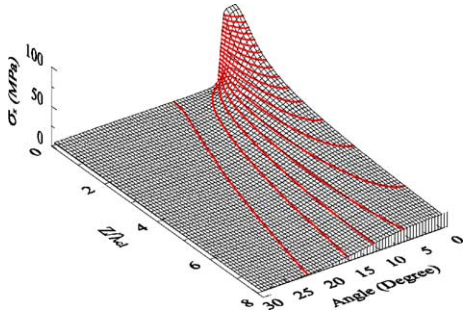

Fig. 15. Distribution of the meridional membrane stress in the cylinder under partial axial compression with $2\theta_n = 5°$.

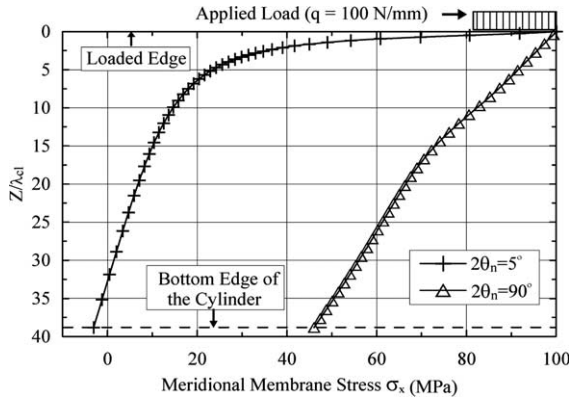

Fig. 16. Meridional membrane stress distributions down the meridian beneath Point A.

the nonlinear buckling mode of the perfect shell are shown in Fig. 17 for several load angles. The peak displacement of the nonlinear eigen-vector (NBM) is near the axial coordinate $Z = 0.6\lambda_{cl}$ for $2\theta_n = 2°$, and 5° and near $Z = 2\lambda_{cl}$ for $2\theta_n = 10°$, 30°, 90° and 150°. If the weld depression is placed at these locations, the largest load reduction due to a weld depression may be expected.

The influence of the weld depression location d on the buckling strength found from GNIA analysis is shown in Fig. 18. For very local loads (small subtended angles θ_n), the imperfection sensitivity curve

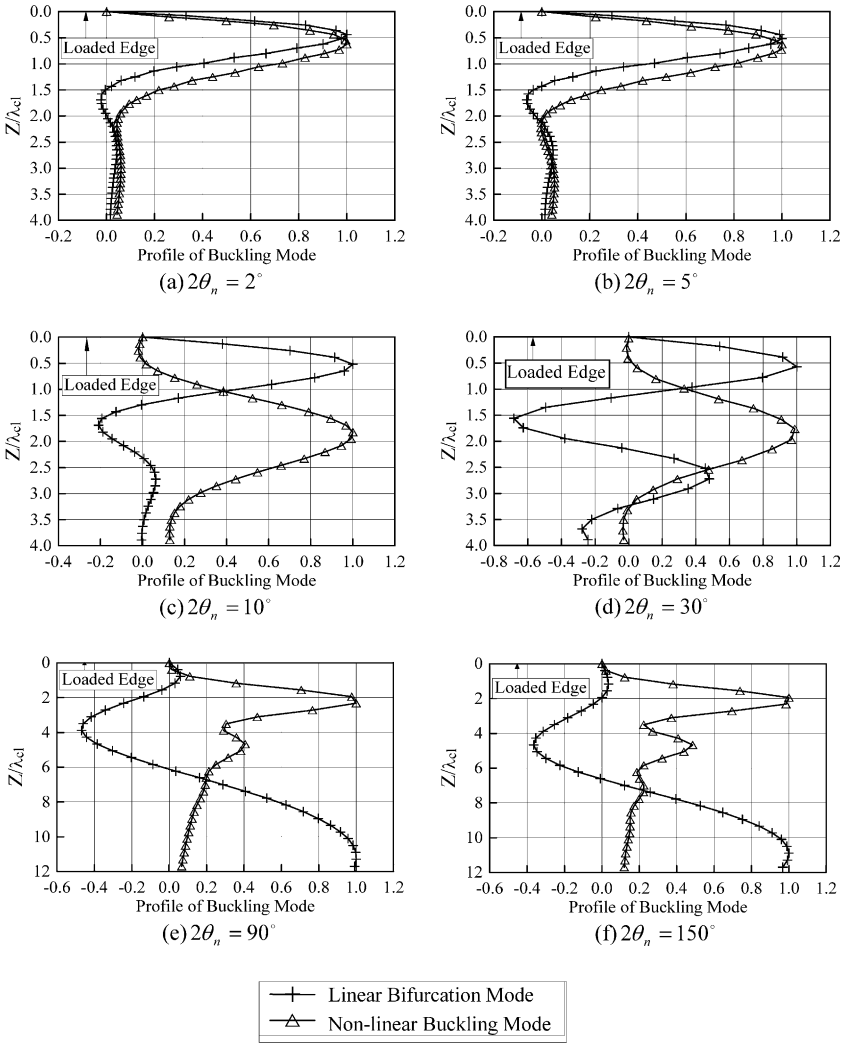

Fig. 17. Axial profiles of buckling modes of the perfect cylinder.

stabilises rapidly with increasing amplitude, and is lowest for positions close to the edge. For large load angles, the imperfection sensitivity curve drops steeply with increasing amplitude, and although it is relatively insensitive to the distance d, the lowest curve supports the above location hypothesis except when $2\theta_n = 10°$. Even for this exceptional case, the hypothesis is not strongly violated as a weld depression at the location of the peak displacement of the nonlinear eigen-vector leads to buckling loads which are similar to those for a weld depression at the worst of the three locations explored. An imperfection location closer than $d = \lambda_{cl} = 0.71\lambda_b$ was not used in Fig. 18 because it would induce a rather large load eccentricity δ_e as shown in Fig. 14.

To ensure that low buckling strengths are not the result of a local load eccentricity δ_e, it was decided to limit the investigation to conditions in which $\delta_e < 0.05\delta$ (Fig. 14). This requirement is satisfied for the Type A depression if the imperfection is located further than $d = 0.55\lambda$ from the edge, where λ is the half-wavelength of the imperfection form. This restriction does not affect the calculations for large angle partial

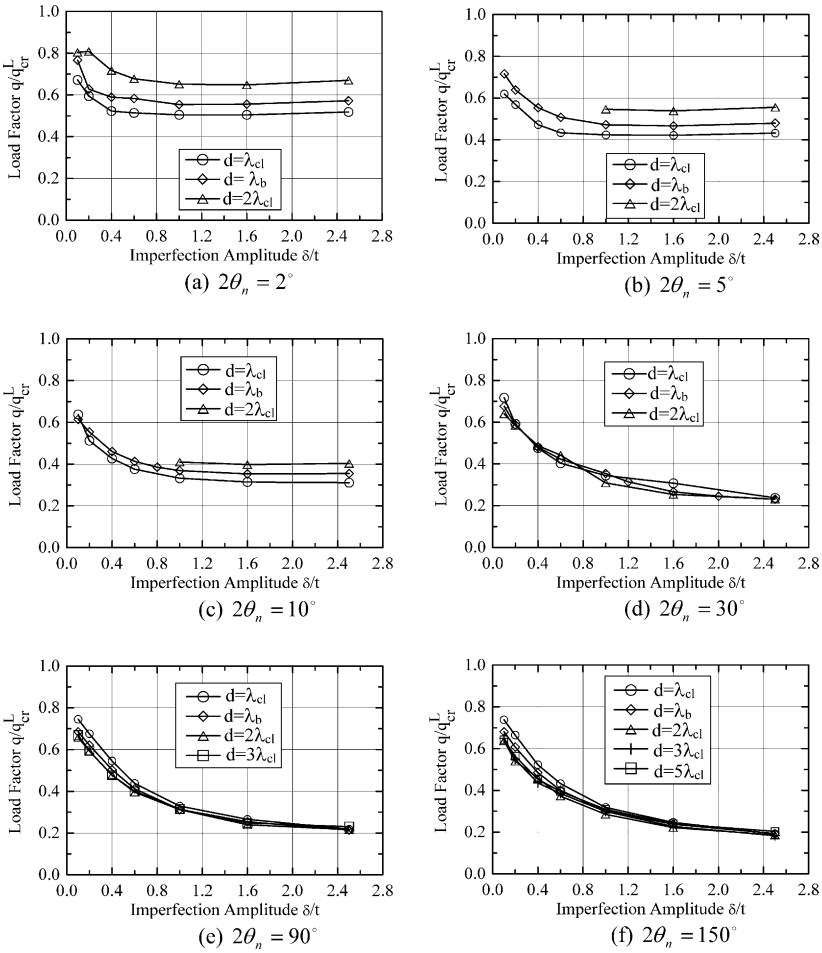

Fig. 18. Imperfection sensitivity curves for WD imperfections with half-wavelength $\lambda = \lambda_b$, located at different distances d from the loaded edge.

loads, but for small subtended angles, the lowest strengths shown in Fig. 18 are for the closest location $d = 0.71\lambda_b$, so closer locations should be explored. To address this problem, calculations were conducted with the half-wavelength λ reduced to $\lambda_b/2$, so that the location $d = 0.6\lambda_{cl}$ indicated by the nonlinear post-buckling mode could satisfy the eccentricity limitation. Since this wavelength $\lambda_b/2$ is rather short, higher strengths may result, but this change permits the sensitivity to location to be explored.

The buckling strengths of shells with this shortened wavelength weld depression are shown in Fig. 19. The lowest strengths can be seen to occur for locations around $d = 0.6\lambda_{cl}$, as suggested by the nonlinear buckling mode. Thus all the calculations of Figs. 18 and 19 indicate that the maximum radial displacement in the nonlinear buckling mode provides a good estimate of the most detrimental location for a weld depression.

5.5.2. *Influence of weld depression wavelength*

The influence of the wavelength of the weld depression was next explored for a fixed weld location at $d = \lambda_b$. The results (Fig. 20) show similar effects to those for uniformly compressed cylinders. At large

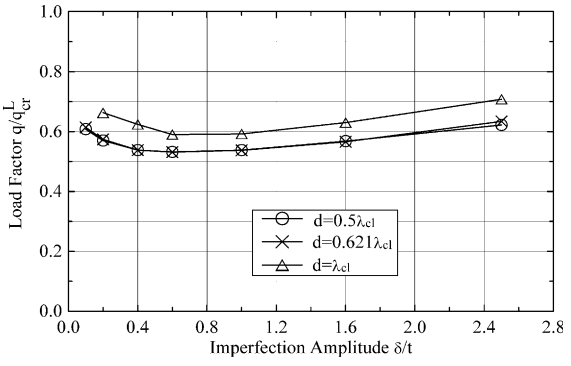

(a) $2\theta_n = 2^\circ$

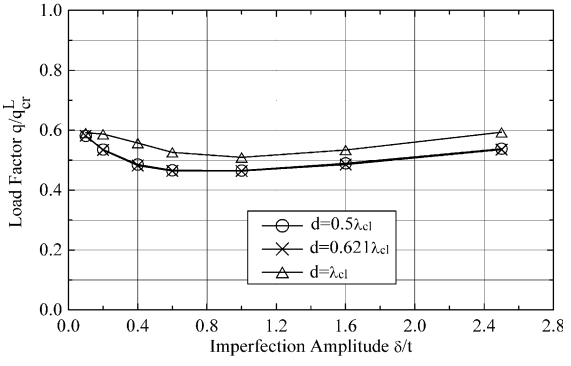

(b) $2\theta_n = 5^\circ$

Fig. 19. Imperfection sensitivity curves for WD imperfections with half-wavelength $\lambda = \lambda_b/2$, located at different distances d from the loaded edge.

amplitudes, longer wavelength imperfections are certainly more detrimental for all partial load angles. However, the most classical axisymmetric critical wavelength ($\lambda = \lambda_{cl}$) is really never critical for this load case. In all subsequent analyses, it was assumed that $\lambda = \lambda_b$, which is consistent with the original rationally based half-wavelength used for Type A weld depression (Rotter and Teng, 1989).

5.6. Comparisons of imperfection sensitivity for different imperfection forms

To obtain a comprehensive picture, a parametric study was carried out employing imperfections of the four above types: the linear bifurcation mode (LBM), the nonlinear buckling mode (NBM), the post-buckling deformed shapes (PDS), and the Type A weld depression (WD). The results are summarised in Fig. 21 for several partial load angles ($2\theta_n = 2°$, 5°, 10°, 30°, 90° and 150°). For the LBM and NBM imperfections, the lower of the inward and outward imperfection buckling strengths is shown. For the PDS imperfection, the lower bound on the 'Max', 'Mid' and 'Min' imperfection forms is shown. Most of the buckling loads of imperfect shells shown in Fig. 21 are limit point loads, but a small number of them are nonlinear bifurcation loads.

The imperfection sensitivity curve obtained by Rotter and Teng (1989) for Type A weld depressions in cylindrical shells under uniform axial compression is also shown in Fig. 21. A comparison of this curve with those for cylinders under wide partial axial loads indicates that their imperfection sensitivities are very similar.

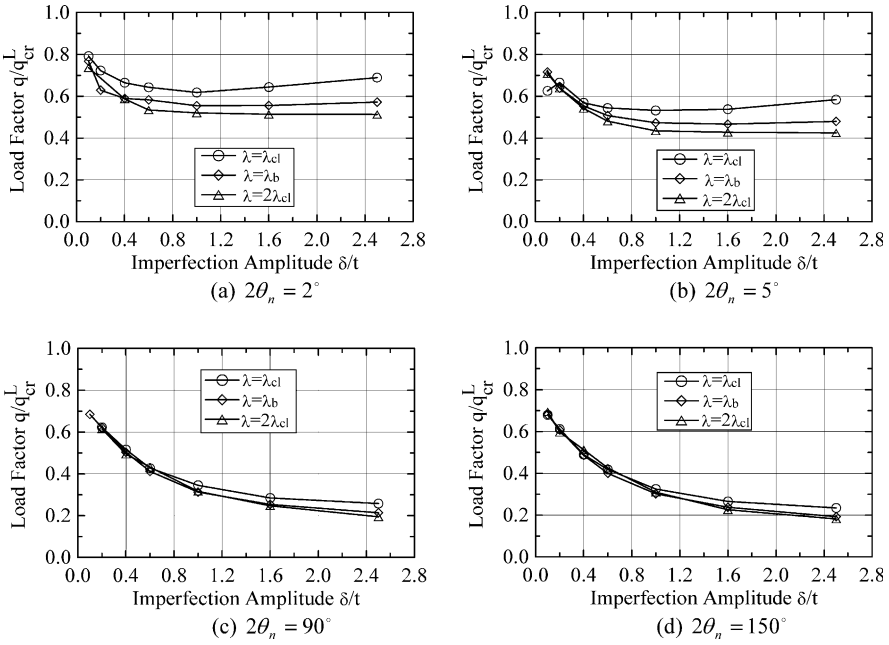

Fig. 20. Imperfection sensitivity curves for WD imperfections with different half-wavelengths λ, located at $d = \lambda_b$ from the loaded edge.

For shells subject to highly localized compression (small angles θ_n), LBM and NBM imperfections have similar effects. But when the loaded zone becomes larger, these two imperfection types have different consequences. When the amplitude is small, NBM imperfections are more severe than LBM imperfections, but as the amplitude is increased, the situation is reversed. It seems that neither the linear bifurcation mode nor the nonlinear buckling mode is universally more detrimental than the other.

For highly localised compression (small angles θ_n), imperfections in the form of the post-buckling deformed shapes (PDS) are the most detrimental of the three types derived from calculation (LBM, NBM and PDS) (Fig. 21). However, as the load angle increases, the situation becomes complicated. Strength curves derived from the three imperfection forms cross over each other throughout the imperfection amplitude range; none dominates over the others. When the imperfection amplitudes are greater than one shell thickness, a condition that is common in real structures, the nonlinear buckling mode (NBM) is never critical as an imperfection form, and it can be discarded without risk.

By contrast, when the imperfection amplitudes are relatively large, the weld depression always has the most detrimental influence on the strength. Moreover, for shells subject to loads with large angles θ_n, the weld depression is the most detrimental for all imperfection amplitudes. For shells under loads with small angles θ_n, the difference between the strength for a weld depression and that for other imperfection forms is small for most amplitudes in many load angles. It should be remembered that the very worst wavelength λ and worst distance d were not employed for these weld depressions: $\lambda = \lambda_b$ and $d = \lambda_{cl}$ or λ_b were adopted. If both factors had been chosen to minimize the buckling load, the effect of weld depressions would have been slightly more detrimental. These calculations demonstrate conclusively that the weld depression can be considered the 'worst' equivalent imperfection form for cylindrical shells under partial axial compression. Only the PDS at small amplitudes is occasionally more detrimental.

The complexity of the imperfection-sensitivity curves (Fig. 21) can be understood in terms of differences between the imperfection forms. For highly localised loads ($2\theta_n = 2^\circ$ and 5°), the linear bifurcation mode and the nonlinear buckling mode are very similar, but the post-buckling deformed shape (PDS), usually in

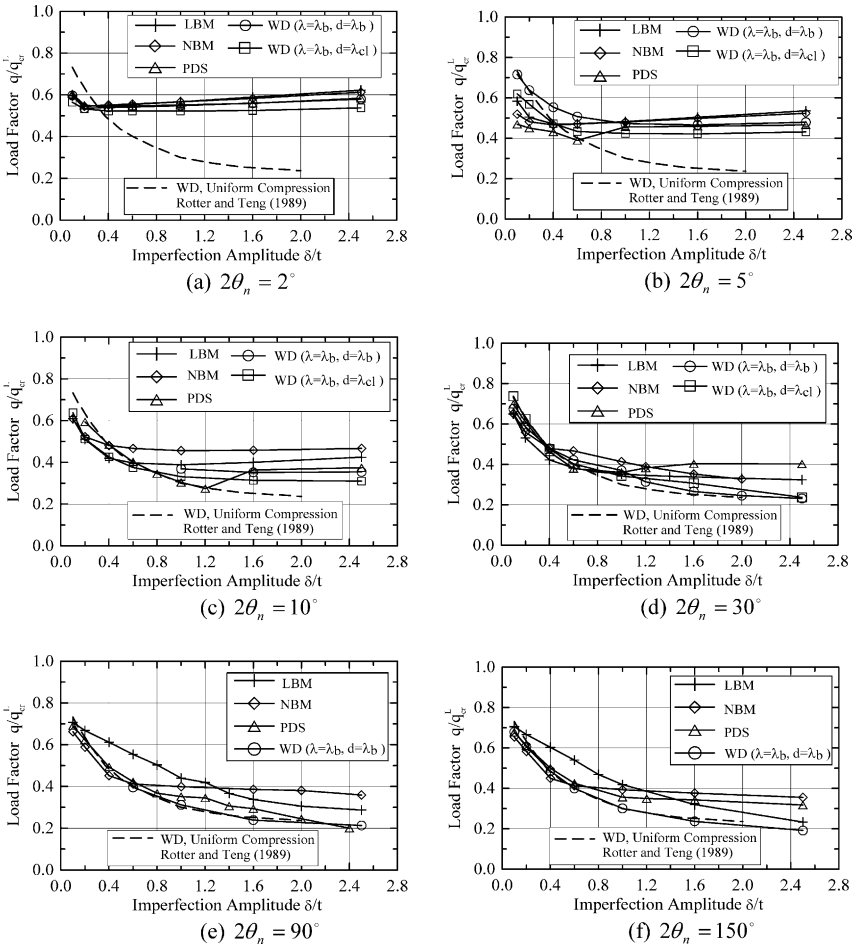

Fig. 21. Comparison of imperfection sensitivity curves for different forms of geometric imperfection.

the form of a dent below the load, is quite different from these buckling modes. This difference is reflected in the imperfection sensitivity curves. For large load angles (e.g. $2\theta_n = 90°$) the three imperfection forms are quite different. The LBM has a long wavelength, strongly affected by the shear stress: the NBM is more localized, though the shear stress effect is still clear. By contrast, the PDS causes two dimples below the loaded edge. The position of these dimples changes as the post-buckling deformation evolves. These significant differences between the imperfection forms lead to substantially different imperfection sensitivity curves.

6. Conclusions

A comprehensive study of the imperfection sensitivity of cylindrical shells under partial axial compression has been presented. Four different imperfection forms have been considered: the linear bifurcation mode (LBM), the nonlinear buckling mode (NBM), several post-buckling deformed shapes (PBS) and local weld depressions (WD).

It has been demonstrated that the linear bifurcation mode is far from being the 'worst' imperfection form for this load case. The nonlinear buckling mode, which for the present cylindrical shell under partial axial compression is the incremental mode of deformation at the limit point load from a GNA analysis of the perfect geometry, is often very different from the linear bifurcation mode. Imperfections in the form of the nonlinear buckling mode have a similar effect to that of imperfections in the form of the linear bifurcation mode: they generally do not lead to the lowest buckling loads either. The effect of imperfections reproducing various post-buckling deformed shapes is also similar.

By contrast, imperfections in the form of weld depressions, which is a realistic form in welded constructions, generally cause the lowest buckling load for realistically large imperfection amplitudes. Weld depressions may therefore be considered to be the most detrimental of these four imperfection forms for cylindrical shells under partial axial compression. It should be noted that the effect of a weld depression depends on its position and wavelength: the results presented here indicate that the critical wavelength may be taken as the linear bending half-wavelength and the critical position can be identified with moderate accuracy from the largest excursion in the nonlinear buckling mode. It has also been shown that the imperfection-sensitivity of cylinders with weld depression imperfections under partial axial compression is similar to that of cylinders under uniform axial compression if the partial load covers a circumferential distance greater than about twice the linear meridional bending half-wavelength.

Acknowledgements

The work described here forms part of the project "Buckling Strength of Steel Cylindrical Shells under a General State of Non-uniform Stresses" funded by the Research Grants Council of the Hong Kong SAR (Project No. PolyU 5081/97E), with additional support from The Hong Kong Polytechnic University. The authors are grateful to both organizations for their financial support.

References

Antoine, P.A., 2000. Comportement des coques cylindriques minces sous chargements combinés: vers une amélioration du dimensionnement sous flexion et pression interne. (Behavior of thin cylindrical shells under combined loading: towards an improved design process for bending and internal pressure), PhD thesis, INSA de Lyon, Lyon, France.

Berry, P.A., Rotter, J.M., Bridge, R.Q., 2000. Compression tests on cylinders with circumferential weld depressions. J. Engrg. Mech., ASCE 126 (4), 405–413.

Cai, M., Holst, J.M.F.G., Rotter, J.M., 2002. Buckling strength of thin cylindrical shells under localised axial compression. In: Proceedings of 15th ASCE Engineering Mechanics Conference, June 2–5, Columbia University, New York, NY, pp. 99–100.

Cai, M.J., Holst, J.M.F.G., Rotter, J.M., 2003. Buckling of cylindrical tank shells under local axial compression stresses. In: Proceedings of International Conference on Design, Inspection and Maintenance of Cylindrical Steel Tanks and Pipelines, Prague, Czech Republic, October 9–11, 2003, pp. 70–76.

Ding, X.L., Coleman, R.D., Rotter, J.M., 1996. Technique for precise measurement of large-scale silos and tanks. J. Survey. Engng., ASCE 122 (1), 14–25.

Ellinas, C.P., Croll, J.G.A., 1986. Elastic–plastic buckling design of cylindrical shells subject to combined axial compression and pressure loading. Int. J. Solids Struct. 22 (9), 1007–1017.

ENV1993-1-6, 1999. Eurocode 3: Design of Steel Structures. Part 1–6: General Rules: Strength and Stability of Shells. European Committee for Standardisation, Brussels.

Esslinger, M., Geier, B., 1972. Gerechnete Nachbeulasten als untere Grenze der experimentellen axialen Beulasten von Kresiszylindern. Der Stahlbau 41 (12), 353–360.

Flügge, W., 1973. Stresses in Shells, second ed. Springer-Verlag, Berlin.

Greiner, R., Derler, P., 1995. Effect of imperfections on wind-loaded cylindrical shells. Thin-Walled Struct. 23, 271–282.

Guggenberger, W., 1992. Nichtlineares Beulverhalten von Kreiszylindrischalen unter lokaler Axialbelastung, Dr. techn dissertation, Institut für Stahlbau, Holzbau und Flächentragwerke, Technische Universität Graz, Austria.

Guggenberger, W., Greiner, R., Rotter, J.M., 2000. The behavior of locally-supported cylindrical shells: unstiffened shells. J. Construct. Steel Res. 56, 175–197.

Hibbit, Karlsson, Sorensen, 1998. ABAQUS/Standard Theory and User's Manuals.

Holst, J.M.F.G., Rotter, J.M., Calladine, C.R., 2000. Imperfections and buckling in cylindrical shells with consistent residual stresses. J. Construct. Steel Res. 54, 265–282.

Koiter, W.T., 1945. On the stability of elastic equilibrium (in Dutch), PhD Thesis, Delft University (see also Translation AFFDL-TR-70-25 Wright Patterson Air Force Base, 1970).

Koiter, W.T., 1963. The effect of axisymmetric imperfections on the buckling of cylindrical shells under axial compression. In: Proceedings, Kon Ned Akad. Wet., Proceedings Ser. B66, pp. 265–279. (See also Appl. Mech. Rev., 18, Review 3387, 1965).

Libai, A., Durban, D., 1977. Buckling of cylindrical shells subjected to nonuniform Axial loads. J. Appl. Mech., ASME 44 (4), 714–720.

Lundquist, E.E., 1935. Strength tests of thin-walled Duralumin cylinders in combined transverse shear and bending, NACA Technical Note No. 523, NASA, Washington.

MacNeal, R., 1994. Finite Elements: Their Design and Application. Marcel Dekker, New York.

Peter, J., 1974. Zur Stabilität von Kreiszylinderschalen unter ungleichmassig verteilten axialen Randbelastungen, Dissertation, Univ Hannover.

Pircher, M., Berry, P.A., Ding, X., Bridge, R.Q., 2001. The shape of circumferential weld-induced imperfections in thin-walled steel silos and tanks. Thin-Walled Struct. 39 (12), 999–1014.

Pircher, M., Bridge, R.Q., 2001a. The influence of circumferential weld-induced imperfections on the buckling of silos and tanks. J. Construct. Steel Res. 57 (5), 569–580.

Pircher, M., Bridge, R.Q., 2001b. Buckling of thin-walled silos and tanks under axial load-Some new aspects. J. Struct. Engrg., ASCE 127 (10), 1129–1136.

Riks, E., 1979. An incremental approach to the solution of snapping and buckling problems. Int. J. Solids Struct. 15, 529–551.

Riks, E., Rankin, C.C., Brogan, F.A., 1996. On the solution of mode jumping phenomena in thin-walled shell structures. Comput. Methods Appl. Mech. Engng. 136, 59–92.

Rotter, J.M., 1985. Buckling of ground-supported cylindrical steel bins under vertical compressive wall loads. In: Proceedings of Metal Structures Conference, Institution of Engineers Australia, Melbourne, May, pp. 112–127.

Rotter, J.M., 1996. Buckling and collapse in internally pressurised axially compressed silo cylinders with measured axisymmetric imperfections: Imperfections, residual stresses and local collapse. In: Proceedings of International Workshop on Imperfections in Metal Silos: Measurement, Characterisation, and Strength Analysis, BRITE/EURAM CA-Silo, Lyon, France, pp. 119–139.

Rotter, J.M., 1997. Pressurised axially compressed cylinders. In: Proceedings of International Conference on Carrying Capacity of Steel Shell Structures, Brno, October 1–3, pp. 354–360.

Rotter, J.M., 1998. Shell structures: the new European standard and current research needs. Thin-Walled Struct. 31 (1–3), 3–23.

Rotter, J.M., 2002. Shell buckling and collapse analysis for structural design: the new framework of the European standard. In: Drew, H.R., Pellegrino, S. (Eds.), New Approaches to Structural Mechanics, Shells and Biological Structures. Kluwer Academic Publishers, London, pp. 355–378.

Rotter, J.M., 2004. Buckling of cylindrical shells under axial compression. In: Teng, J.G., Rotter, J.M. (Eds.), Buckling of Thin Metal Shells. Spon Press, London, pp. 42–87.

Rotter, J.M., Coleman, R., Ding, X.L., Teng, J.G., 1992. The measurement of imperfections in cylindrical silos for buckling strength assessment. In: Proceedings of Fourth International Conference on Bulk Materials Storage Handling and Transportation, Institution of Engineers, Australia, Wollongong, June 1992, pp. 473–479.

Rotter, J.M., Teng, J.G., 1989. Elastic stability of cylindrical shells with weld depressions. J. Struct. Engrg., ASCE 115 (5), 1244–1263.

Saal, H., 1982. Buckling of long liquid-filled cylindrical shells. In: Ramm, E. (Ed.), Buckling of Shells. Springer-Verlag.

Schneider, W., Höhn, K., Timmel, I., Thiele, R., 2001. Quasi-collapse-affine imperfections at slender wind-loaded cylindrical steel shells. In: Proceedings of 2nd European Conference on Computational Mechanics—ECCM-2001, Cracow, Poland.

Seide, P., Weingarten, V.I., 1961. On the buckling of circular cylindrical shells under pure bending. J. Appl. Mech., ASME 28 (1), 112–116.

She, K.M., Rotter, J.M., 1993. Nonlinear and stability behavior of discretely-supported cylinders, Research Report 93-01, Department of Civil Engineering, University of Edinburgh.

Song, C.Y., 2002. Buckling of shells under non-uniform stress states, PhD Thesis, Department of Civil and Structural Engineering, The Hong Kong Polytechnic University.

Speicher, G., Saal, H., 1991. Numerical calculation of limit loads for shells of revolution with particular regard to the applying equivalent initial imperfections. In: Jullien, J.F. (Ed.), Buckling of Shell Structures, on Land, in the Sea and in the Air. Elsevier Applied Science, London, pp. 466–475.

Stephens, W.B., Starnes Jr., J.H., 1975. Collapse of long cylindrical shells under combined bending and pressure loads. AIAA J. 13 (1), 20–25.

Teng, J.G., 1996. Buckling of thin shells: recent advances and trends. Appl. Mech. Rev., ASME 49 (4), 263–274.

Teng, J.G., Rotter, J.M., 1992. Buckling of pressurized axisymmetrically imperfect cylinders under axial loads. J. Engrg. Mech., ASCE 118 (2), 229–247.

Teng, J.G., Rotter, J.M. (Eds.), 2004. Buckling of Thin Metal Shells. Spon Press, London.

Teng, J.G., Song, C.Y., 2001. Numerical models for nonlinear analysis of elastic shells with eigenmode-affine imperfections. Int. J. Solids Struct. 38 (18), 3263–3280.

Tennyson, R.C., Muggeridge, D.B., 1969. Buckling of axisymmetric imperfect circular cylindrical shells under axial compression. AIAA J. 7 (11), 2127–2131.

Timoshenko, S.P., Gere, J.M., 1963. Theory of Elastic Stability, second ed. McGraw-Hill Book Company.

Yamaki, N., 1984. Elastic Stability of Circular Cylindrical Shells. North Holland, Elsevier Applied Science Publishers, Amsterdam.